Journal of Magnetic Resonance 203 (2010) 144–149

Contents lists available at ScienceDirect

Journal of Magnetic Resonance

journal homepage: www.elsevier.com/locate/jmr

Homonuclear dipolar decoupling under fast MAS: Resolution patterns and simple optimization strategy

Kanmi Mao, Marek Pruski *

Ames Laboratory, Iowa State University, Ames, IA 50011-3020, USA
Department of Chemistry, Iowa State University, Ames, IA 50011-3020, USA

ARTICLE INFO

Article history:
Received 14 November 2009
Revised 14 December 2009
Available online 22 December 2009

Keywords:
Solid-state NMR
Fast MAS
CRAMPS
Homonuclear decoupling
PMLG
Optimization

ABSTRACT

A simple method is shown for optimization of ^{1}H homonuclear dipolar decoupling at MAS rates exceeding 10 kHz. By monitoring the intensity of a spin-echo under the decoupling conditions, it is possible to optimize the amplitude of the RF magnetic field, the cycle time of the decoupling sequence and the resonance offset within minutes. As a result, the decoupling efficiency can be quickly and reliably fine-tuned without using a reference sample. The utility of this method has been confirmed by studying the resolution patterns for the supercycled PMLG scheme, which were found to be in excellent agreement with earlier theoretical predictions and verified in high-resolution 2D ^{1}H–^{1}H experiments.

1. Introduction

Overcoming the strong homonuclear dipolar interactions between ^{1}H nuclei has been one of the principal pursuits in solid-state NMR spectroscopy for several decades. The advancement of high-resolution ^{1}H NMR in solids commenced with the introduction of Lee–Goldburg (LG) RF decoupling [1] and was followed by the development of multiple-pulse sequences for static samples [2–4]. The first highly resolved ^{1}H spectra were attained by combining these sequences with slow magic angle spinning (MAS), to eliminate the chemical shift anisotropy (CSA), in an experiment referred to as CRAMPS (combined rotation and multiple-pulse sequence) [5]. Subsequently, improved RF schemes emerged that enabled high-resolution ^{1}H NMR at MAS rates up to 25 kHz, which included frequency-switched LG (FSLG) [6], phase-modulated LG (PMLG) [7], decoupling using mind-boggling optimization (DUMBO) [8] and symmetry-based (R-based and smooth amplitude modulation, SAM) [9,10] pulse sequences. In depth theoretical analyses of most of these experiments were offered based on the average Hamiltonian theory [11,12] and the Floquet theory [13,14]. It has been generally implied that the homonuclear decoupling sequences perform well under the so-called 'quasi-static condition', where the sample spinning period $\tau_R = (\nu_R)^{-1}$ is long relative to the cycle time of the RF sequence τ_c. However, the development of ultra fast MAS [15], which can now reach frequencies in the range $40 \leqslant \nu_R \leqslant 70$ kHz, induced interest in application of homonuclear decoupling under conditions that can no longer be 'quasi-static' under practical RF amplitudes. Most recently, the windowed and windowless PMLG, DUMBO and SAM schemes were shown to perform surprisingly well in the regime where τ_R and τ_c are comparable (but not equal), both in terms of resolution [16,17] and sensitivity [17], and theoretical arguments were presented that rationalize the experimentally observed resolution patterns [18]. These findings open new opportunities for designing two- and three-dimensional (2D and 3D) correlation experiments, which involve at least one ^{1}H dimension with CRAMPS-quality resolution and utilize the spectral range, sensitivity and RF flexibility offered by fast MAS probes.

In spite of the importance of the homonuclear decoupling techniques, their widespread use by the scientific community has been affected by the experimental challenges involved in the setup and optimization. Early CRAMPS experiments, which used homebuilt RF circuitry and probes, were intricate due to rigorous requirements on pulse shapes, phases, timing and RF homogeneity [19,20]. Extensive analyses have been dedicated to the practical aspects of the currently used PMLG and DUMBO sequences. Although the difficulties due to RF imperfections and instabilities have been largely overcome in present-day spectrometers, practical implementation of ^{1}H homonuclear decoupling remains demanding and time consuming. The performance of state-of-the-art sequences is defined by a number of parameters, most of which are difficult to predict a priori. In particular, the optimum RF amplitude for PMLG decoupling does not necessarily correspond to the

* Corresponding author. Fax: +1 515 294 5233.
E-mail address: mpruski@iastate.edu (M. Pruski).

1090-7807/$ - see front matter © 2009 Elsevier Inc. All rights reserved.
doi:10.1016/j.jmr.2009.12.013

LG condition [18,21]. More importantly, the decoupling deteriorates rapidly when the ratio $\psi = \nu_c/\nu_R$ (where $\nu_c = (\tau_c)^{-1}$) is near the so-called degeneracy conditions $n\nu_c = m\nu_R$ (n, $m = 1, 2, \ldots$). The limitations imposed by these conditions on the experimental parameters strongly depend on the MAS rate [18].

One of the optimization strategies relies upon monitoring the effect of ^{1}H decoupling on ^{13}C spectra, e.g. of adamantane or alanine [6,22,23]. The suppression of ^{1}H homonuclear dipolar interactions renders the ^{1}H–^{13}C spin pairs equivalent to the AX system in solution [24,25], providing a sensitive probe of the decoupling efficiency and a good estimate of the scaling factor through the observation of J-multiplets. A more direct method involves acquisition of high-resolution 1D or 2D ^{1}H–^{1}H spectra of a reference sample, usually glycine, which allows for optimization of the amplitude of the RF magnetic field ν_{RF} and the τ_c/τ_R ratio [13,17,18,21,22,26,27], calibration of the effective field [26] and the scaling factor [23,26,27], optimization of the resonance offset, the pulse imperfections and the spectral artifacts [13,21,27,28].

Recently, we studied the utility of ^{1}H decoupling under fast MAS in ^{13}C and ^{1}H-detected through-bond heteronuclear correlation (HETCOR) experiments [29], where the best performance of PMLG and SAM3 sequences was found by minimizing the loss of signal due to transverse relaxation (T_2') in a simple spin-echo experiment. Here, we will demonstrate that this strategy is of general practical relevance to high-resolution ^{1}H spectroscopy. By monitoring the

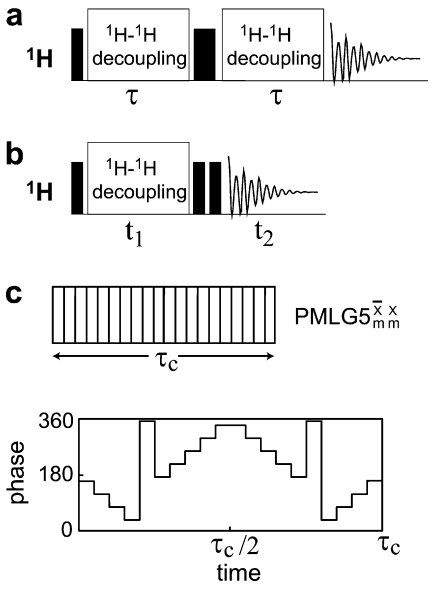

Fig. 1. Pulse sequences for (a) spin-echo experiment with PMLG5$^{\bar{x}x}_{mm}$ ^{1}H homonuclear decoupling during τ, (b) 2D ^{1}H–^{1}H correlation experiment using PMLG5$^{\bar{x}x}_{mm}$ decoupling in the indirect dimension, and (c) schematic representation of the PMLG5$^{\bar{x}x}_{mm}$ block.

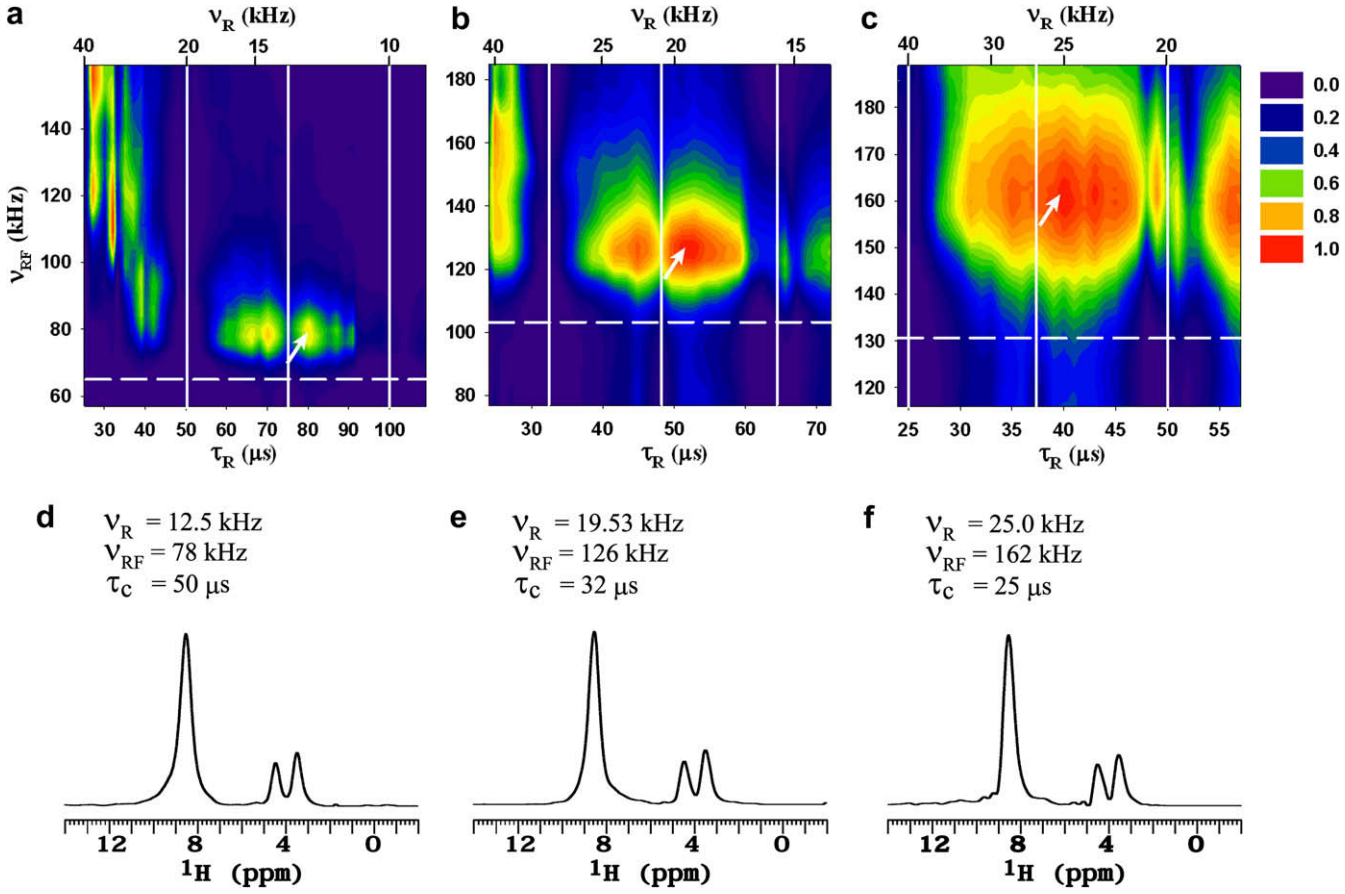

Fig. 2. The integrated intensity of spin-echo in glycine as a function of τ_R and ν_{RF}, measured under PMLG5$^{\bar{x}x}_{mm}$ decoupling, with $\tau \cong 2$ ms, the carrier frequency set at 4 ppm from TMS, and $\tau_c = 50$ μs (a), 32 μs (b) and 25 μs (c). The experiments were performed at 14.1 T on a Varian NMR System 600 MHz spectrometer, equipped with 1.6 mm triple-resonance MAS probe. The plots comprise 2000 points representing integrated intensity of the entire echo signal measured for 40 values of τ_R and 50 values of ν_{RF}. Each signal consisted of 4 scans acquired using acquisition delay of 2 s. The measurement took approximately 3 days per plot. The contours were normalized relative to the highest intensity observed in each plot. The vertical lines correspond from left to right to $\psi = 1$, 3/2 and 2. The dashed line represents the LG value $\nu_{RF,LG} = 4\sqrt{2/3}\nu_c$. (d–f) The projections of indirect dimensions of 2D ^{1}H–^{1}H correlation spectra measured using the ν_R and ν_{RF} values indicated by arrows in (a–c). Each spectrum was acquired in 160 rows, 8 scan per row, with t_1 increment of ~100 μs, and the total experiment time was 1.5 h.

echo intensity for a fixed delay τ, it is possible to quickly and reliably navigate through the complex space of experimental parameters and gauge the decoupling efficiency of the supercycled PMLG scheme as a function of ν_{RF}, ν_R, ν_c, and the resonance offset without acquiring high-resolution spectra. The observed patterns are compared with those recently calculated by Vega et al. based on the bimodal Floquet theory [18]. We conclude by offering a tuning 'recipe', which affords simple and fast optimization of the homonuclear decoupling using directly the sample of interest.

2. Results and discussion

2.1. Resolution patterns

The pulse sequences for spin-echo and 2D ^{1}H–^{1}H correlation experiments are shown in Fig. 1a and b. All measurements were performed using the supercycled PMLG scheme, denoted PMLG5$^{\bar{x}x}_{mm}$, which consists of two blocks PMLG5$^{x}_{m}$ and PMLG5$^{\bar{x}}_{m}$ with phase rotation as shown in Fig. 1c [30].

The contour plots shown in Fig. 2a–c represent the intensities of spin-echoes observed for glycine (full rotor) using a τ value of approximately 2 ms, the carrier frequency at 4 ppm with respect to TMS, and three different PMLG5$^{\bar{x}x}_{mm}$ cycle periods τ_c of 50 μs (ν_c = 20 kHz), 32 μs (ν_c = 31.25 kHz) and 25 μs (ν_c = 40 kHz). Each plot consists of 2000 data points representing the total echo intensity, including the spinning sidebands, measured for 50 values of ν_{RF} and 40 values of ν_R, the ranges of which are compatible with the theoretical results of Vega et al. (Figs. 2 and 3 in Ref. [18]), within the capabilities of our Varian FastMAS^{TM} probe. The results shown in Fig. 2a–c (as well as those in Fig. 3a and b, below) were obtained using rotor synchronization of τ. Under such conditions, τ is not in general a multiple of τ_c, in which case ^{1}H decoupling

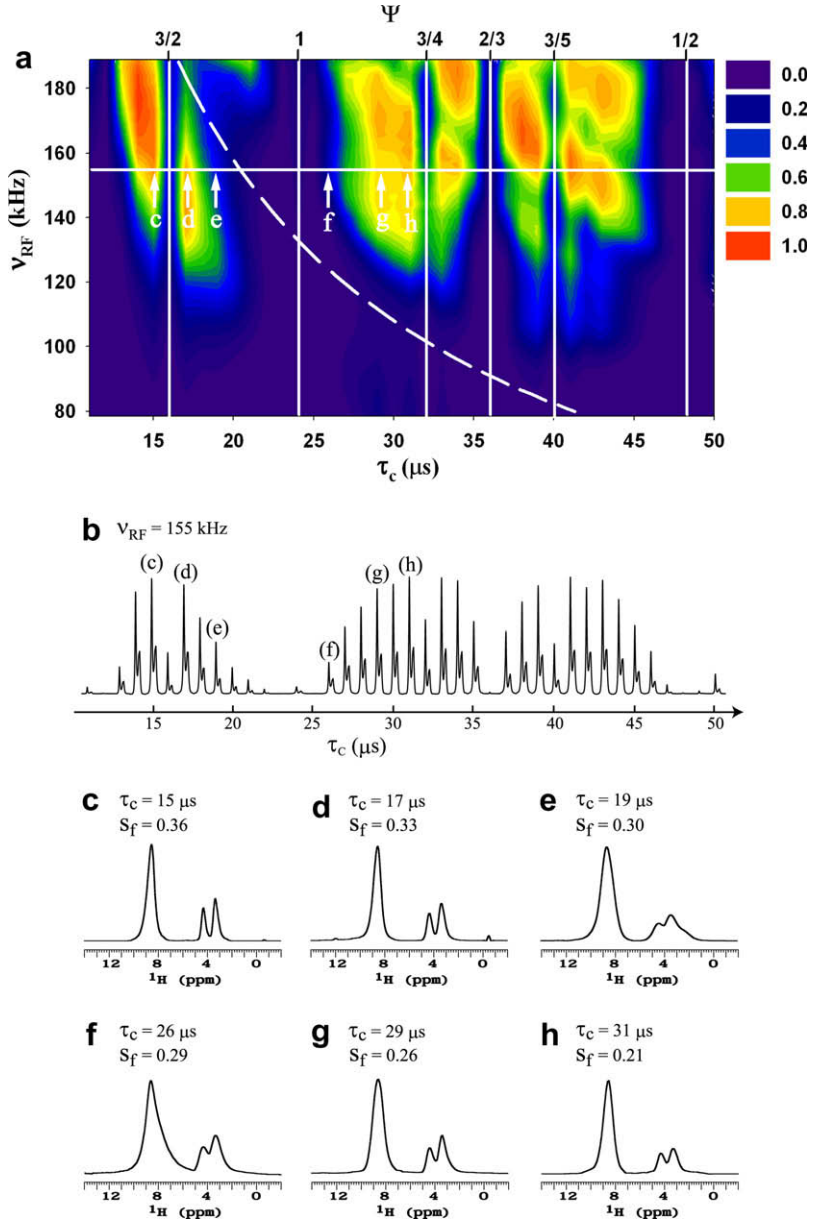

Fig. 3. (a) The integrated intensity of spin-echo in glycine as a function of τ_c and ν_{RF}, measured under PMLG5$^{\bar{x}x}_{mm}$ decoupling, with $\tau \cong 2$ ms and τ_R = 24 μs (ν_R = 41.67 kHz). The plot consists of 1920 points representing integrated intensity of the entire echo signal measured for 40 values of τ_c and 48 values of ν_{RF}. The dashed curve corresponds to the LG condition $\nu_{RF,LG}$ and the vertical lines to ψ = 3/2, 1, 3/4, 2/3, 3/5 and 1/2. The measurement time was approximately 4 h. (b) A series of 1D spectra measured for ν_{RF} = 155 kHz (horizontal line in (a)). (c–h) The projections of 2D ^{1}H–^{1}H correlation spectra obtained under decoupling conditions marked in (a) and (b). Other experimental conditions were as given in the caption to Fig 2.

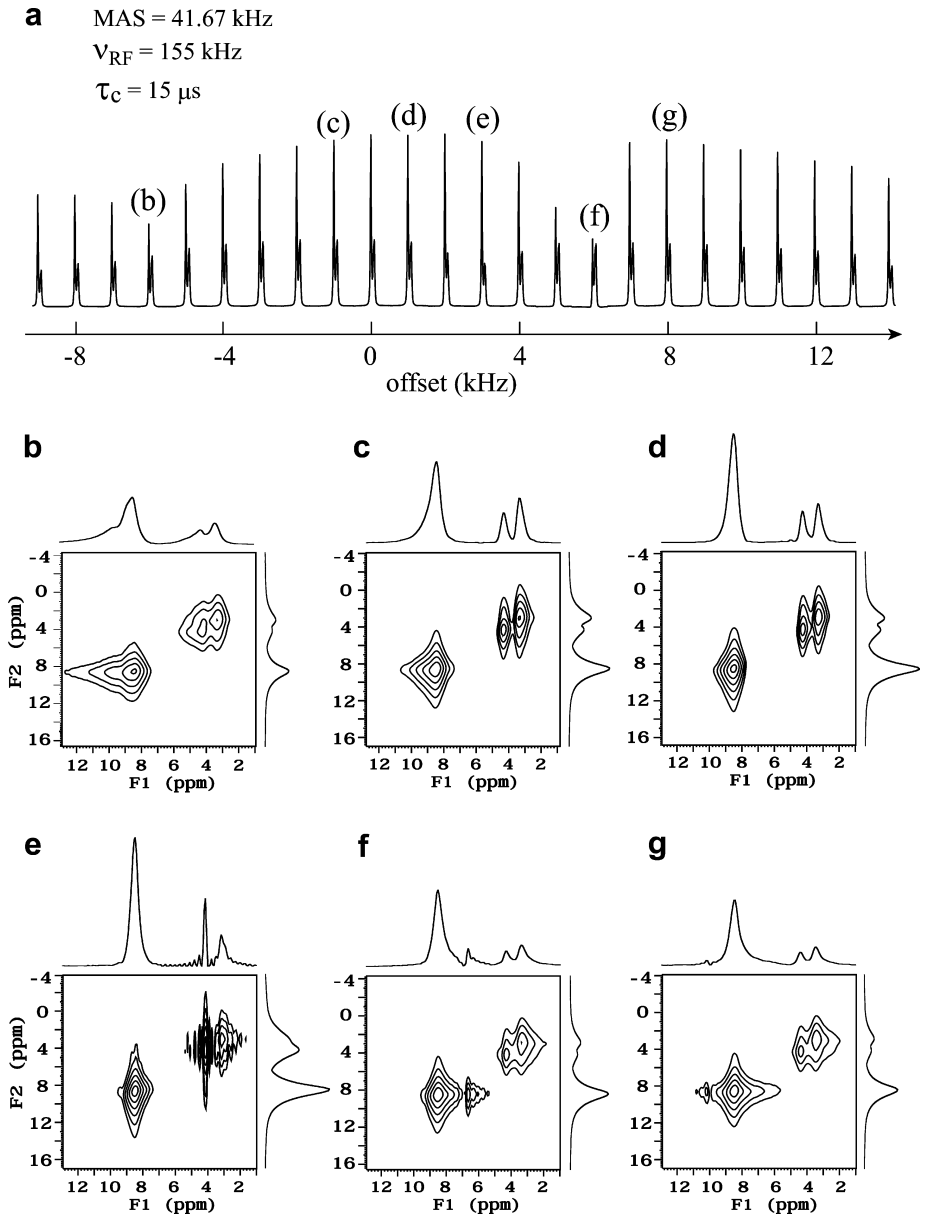

Fig. 4. (a) The spin-echo spectra of glycine as a function of resonance offset with respect to the carrier frequency used in previous measurements, set at 4 ppm from TMS. The experimental parameters were the same as for the spectrum shown in Fig. 3c, which corresponds to offset equal zero. (b–g) 2D ^{1}H–^{1}H correlation spectra measured under decoupling conditions marked in (a). Other experimental conditions were as given in the caption to Fig 2.

is 'off' for a fraction of the rotor period on each side of the π pulse. During these 'off' periods, which vary with τ_R and τ_c, ^{1}H magnetization evolves only under MAS. We should point out that the resulting dephasing is insignificant at high MAS rates. Indeed, we have verified that at ν_R = 20 and 40 kHz the spin-echo patterns observed with and without rotor synchronization were indistinguishable. As noted in Section 2.2, at $\nu_R \leqslant 10$ kHz, the non-synchronized patterns were in fact more reliable, at least in the glycine sample studied here.

There are clear similarities between the experimental and theoretical patterns. The left and right vertical lines in Fig. 2a–c, which correspond to $\psi = 1$ (i.e. $\nu_c = \nu_R$) and 2 ($\nu_c = 2\nu_R$) correspond to areas with the lowest echo intensity. The same areas were identified as most sensitive to the zero-order degeneracy conditions in the Floquet Hamiltonian. Other such areas correspond to $\psi = 1/2$ and 2/3. These are only represented in Fig. 2a, at τ_R = 25 and 33.3 μs, respectively (not marked). Weak echo intensity has been also observed at $\psi = 3/2$, as indicated by the central vertical line in Fig. 2a–c. This coincides with the region of first-order degeneracy effect, where the decline in PMLG5$^{xx}_{mm}$ decoupling was detected using numerical simulations [18]. Additional 'dips' in echo intensity observed for high MAS rates in Fig. 2a are also due to first-order degeneracies, which are closely spaced for $\psi \leqslant 3/2$ (also see discussion of Fig. 3a, below).

The spectra in Fig. 2d–f represent high-resolution projections of the 2D ^{1}H–^{1}H spectra measured under the conditions indicated by arrows in Fig. 2a–c. Clearly, high quality decoupling has been achieved in all three spectra. These results show that the best refocusing has not been reached under the LG condition $\nu_{RF,LG} = 4\sqrt{2/3}\nu_c$, indicated by the dashed horizontal line in Fig. 2a–c, but at the ν_{RF} values approximately 20% higher. Interestingly, these values are within ±3% of the theoretically determined maxima of decoupling efficiency (Fig. 2a–c in Ref. [18]), which implies that the observed divergence is not due to inaccurate esti-

mate of ν_{RF} or RF inhomogeneity. Note, however, that under MAS at 41.67 kHz, the best resolution was found at $\nu_{RF} < \nu_{RF,LG}$ (see below).

The ψ values of 1.4 and 1.6 appear to be universally reliable, which in the case of fast MAS implies the use of high ν_c as well as high ν_{RF}. The parameter space associated with high echo intensity increases considerably with increasing ν_c, which favors probes with excellent RF capabilities. In general, the decoupling efficiency depends on the proximity of these areas to $\nu_{RF,LG}$. The overall decoupling performance also depends on the scaling factor s_f, which is not discernible in the spin-echo experiment. As expected, the scaling factor is unrelated to ν_R, with ν_c and ν_{RF} being constant. For any given set of ν_c and ν_R, an increase of ν_{RF} lowers the scaling factor. For example, the spectra shown in Fig. 2 have approximately the same value $s_f \cong 0.30$. Spectra of similar quality can be obtained within the 'red area' on the right side of Fig. 2c, whereas the s_f value is considerably reduced for the area of high echo intensity in the upper left part of Fig. 2a.

Additional insights can be obtained by monitoring the echo intensity as a function of τ_c and ν_{RF}, at a constant MAS rate. Fig. 3a represents a contour plot measured at $\nu_R = 41.67$ kHz ($\tau_R = 24$ μs). Note that the slices at $\tau_c = 25$, 32 and 50 μs match up closely with the left vertical edges of Fig. 2a, b and c. The areas of low echo intensity include the entire bottom half of the figure ($\nu_{RF} < 140$ kHz), the vicinity of LG condition, and the vertical strips corresponding to low ψ values of 3/2, 1 (broad region), 3/4, 2/3, 3/5, and 1/2 (broad region).

The set of spectra in Fig. 3b corresponds directly to the horizontal slice at $\nu_{RF} = 155$ kHz (solid line in Fig. 3a). The high-resolution ^{1}H spectra shown in Fig. 3c–h were measured under the conditions designated by (c), (d), (e), (f), (g) and (h) in Fig. 3b (also marked c–h in Fig. 3a). As a general rule, under constant ν_{RF} the scaling factor improves for short τ_c (as noted in Fig. 3c–h), and under constant τ_c for low ν_{RF}, as noted earlier. Overall, the best performance is again observed around $\psi = 1.6$ and 1.4 (Figs. 3c and d), whereas experiments corresponding to low intensity echoes near $\nu_{RF,LG}$ (Fig. 3e) or high intensity echoes further away from $\nu_{RF,LG}$ (Fig. 3h) yield poor ^{1}H resolution.

Finally, we show the effect of the resonance offset on spin-echo intensity and ^{1}H resolution (Fig. 4). Again, the decoupling efficiency can be easily assessed based on the echo intensity, although the effect of offset varies across each spectrum. Small offsets are preferred, which is in agreement with earlier results obtained using windowed PMLG5$^{\bar{x}x}_{mm}$ sequence and MAS rates of 7–14 kHz [27].

2.2. Simple optimization strategy

The measurements shown in Figs. 2 and 3, which took days and hours to acquire, respectively, are not needed in routine optimizations of the decoupling efficiency. The selection of proper experimental parameters (ν_R, ν_{RF}, ν_c and the resonance offset) can be done quickly and reliably by performing a very limited number of spin-echo experiments. The choice of ν_R is usually dictated by the research needs and probe capabilities, and we first assume the use of fast MAS, as required in HETCOR experiments at high magnetic fields. It is clear from Fig. 3a that this implies the use of the strongest available RF field. The best value of ν_c must be correlated with ν_{RF} by the LG condition (roughly) and with ν_R via the constrains imposed by the ψ ratio. We used the following steps:

(i) set ν_{RF} at 80–90% of the maximum 'safe' value for the probe and τ at around 2 ms,
(ii) measure a series of spin-echo spectra as a function of τ_c similar to that shown in Fig. 3b,
(iii) choose the best value of τ_c (see below) and fine-tune ν_{RF} by arraying it around the starting value, and
(iv) use the best values of τ_c and ν_{RF} to optimize the offset, again by collecting a series of echoes.

As noted earlier, under fast MAS step (ii) may be performed with or without rotor synchronization. In the latter case, τ has to be fine-tuned, such that it becomes a multiple of τ_c for each echo in a series. Step (iii) may involve some ambiguity when comparable echo maxima are observed for different values of τ_c, such as those marked (c) and (h) in Fig. 3b. In such case the maximum associated with shorter τ_c is preferred, because it is associated with a higher scaling factor, as indeed confirmed in Fig. 3c and h. A more methodical search can be initially carried out by the repeating steps (ii) and (iii) for several values of ν_{RF}, but it is not needed once the routine is established. In samples studied in our laboratory (glycine, tripeptide f-MLF-OH and a series of coals) these tasks could be performed directly on the sample of interest within 20–30 min and invariably led to excellent resolution.

As Fig. 2 demonstrates, a similar strategy can be applied at lower MAS rates, down to at least 10 kHz. Rotor-synchronization should be avoided under slow MAS because the echo patterns observed as a function of τ_c (step (ii)) may become τ-dependent due to the abovementioned difficulties with timing of the sequence.

3. Conclusion

The spin-echo measurement provides a quick and reliable method for optimization of ^{1}H homonuclear decoupling without using a reference sample. Its utility has been confirmed at MAS rates above 10 kHz by excellent agreement of the observed efficiency patterns of the supercycled Lee–Goldburg sequence with earlier theoretical predictions and verified in high-resolution 2D ^{1}H–^{1}H experiments. For this sequence, the best performance was observed when the ratio $\psi = \nu_c/\nu_R$ was approximately 1.4 or 1.6.

Although further studies are needed in order to better understand the relationship between transverse coherence lifetime of protons and the functioning of homonuclear decoupling, we expect that similar strategy can be used to optimize other sequences, such as SAM and PMLG5^x_m (which we verified, see Ref. [29]) or DUMBO, under windowed and windowless conditions. In sequences where the average Hamiltonian does not generate z-rotation, additional pulses before and after each decoupling block should be used to rotate the ^{1}H magnetization into the xy plane.

Acknowledgment

The authors thank Drs. S. Vega and J.-P. Amoureux for helpful discussions. This research was supported at the Ames Laboratory by the U.S. Department of Energy, Office of Basic Energy Sciences, under Contract No. DE-AC02-07CH11358.

References

[1] M. Lee, W. Goldburg, Nuclear magnetic resonance line narrowing by rotating rf field, Phys. Rev. 140 (1965) A1261–1271.
[2] J.S. Waugh, L.M. Huber, U. Haeberlen, Approach to high-resolution nmr in solids, Phys. Rev. Lett. 20 (1968) 180–183.
[3] W.K. Rhim, D.D. Elleman, R.W. Vaughan, Enhanced resolution for solid state NMR, J. Chem. Phys. 58 (1973) 1772–1773.
[4] D.P. Burum, W.K. Rhim, Analysis of multiple pulse NMR in solids, J. Chem. Phys. 71 (1979) 944–956.
[5] B.C. Gerstein, R.G. Pembleton, R.C. Wilson, L.M.J. Ryan, High resolution NMR in randomly oriented solids with homonuclear dipolar broadening: combined multiple pulse NMR and magic angle spinning, J. Chem. Phys. 66 (1977) 361–362.
[6] A. Bielecki, A.C. Kolbert, M.H. Levitt, Frequency-switched pulse sequences – homonuclear decoupling and dilute spin NMR in solids, Chem. Phys. Lett. 155 (1989) 341–346.
[7] E. Vinogradov, P.K. Madhu, S. Vega, High-resolution proton solid-state NMR spectroscopy by phase-modulated Lee–Goldburg experiment, Chem. Phys. Lett. 314 (1999) 443–450.

[8] D. Sakellariou, A. Leasge, P. Hodgkinson, L. Emsley, Homonuclear dipolar decoupling in solid-state NMR using continuous phase modulation, Chem. Phys. Lett. 319 (2000) 253–260.
[9] P.K. Madhu, X. Zhao, M.H. Levitt, High-resolution ^{1}H NMR in the solid state using symmetry-based pulse sequences, Chem. Phys. Lett. 346 (2001) 142–148.
[10] J.-P. Amoureux, B. Hu, J. Trebosc, Enhanced resolution in proton solid-state NMR with very fast MAS experiments, J. Magn. Reson. 193 (2008) 305–307.
[11] U. Haeberlen, J.S. Waugh, Coherent averaging effects in magnetic resonance, Phys. Rev. 175 (1968) 453–467.
[12] M.H. Levitt, Symmetry in the design of NMR multiple-pulse sequences, J. Chem. Phys. 128 (2008) 052205.
[13] M. Leskes, P.K. Madhu, S. Vega, Supercycled homonuclear dipolar decoupling in solid-state NMR: toward cleaner ^{1}H spectrum and higher spinning rates, J. Chem. Phys. 128 (2008) 052309.
[14] E. Vinogradov, P.K. Madhu, S. Vega, Strategies for high-resolution proton spectroscopy, Top. Curr. Chem. 246 (2004) 33–90.
[15] A. Samoson, T. Tuherm, J. Past, A. Reinhold, T. Anupold, I. Heinmaa, New horizons for magic angle spinning NMR, Top. Curr. Chem. 246 (2005) 15–31.
[16] M. Leskes, S. Steuernagel, D. Schneider, P.K. Madhu, S. Vega, Homonuclear dipolar decoupling at magic angle spinning frequencies up to 65 kHz in solid-state nuclear magnetic resonance, Chem. Phys. Lett. 466 (2008) 95–99.
[17] E. Salager, R.S. Stein, S. Steuernagel, A. Lesage, B. Eléna, L. Emsley, Enhanced sensitivity in high-resolution ^{1}H solid-state NMR spectroscopy with DUMBO dipolar decoupling under ultra-fast MAS, Chem. Phys. Lett. 469 (2009) 336–341.
[18] M. Leskes, P.K. Madhu, S. Vega, Why does PMLG proton decoupling work at 65 kHz MAS?, J Magn. Reson. 199 (2009) 208–213.
[19] B.C. Gerstein, C.R. Dybowski, Transient Techniques in NMR in Solids, Academic, New York, 1985.
[20] C.E. Bronnimann, B.L. Hawkins, M. Zhang, G.E. Maciel, Combined rotation and multiple pulse spectroscopy as an analytical proton nuclear magnetic resonance technique for solids, Anal. Chem. 60 (1988) 1743–1750.
[21] C. Coelho, J. Rocha, P.K. Madhu, L. Mafra, Practical aspects of Lee–Goldburg based CRAMPS techniques for high-resolution ^{1}H NMR spectroscopy in solids: implementation and applications, J. Magn. Reson. 194 (2008) 264–282.
[22] M.E. Stoll, A.J. Vega, R.W. Vaughan, Heteronuclear dipolar modulated chemical shift spectra for geometrical information in polycrystalline solids, J. Chem. Phys. 65 (1976) 4093–4098.
[23] M. Leskes, P.K. Madhu, S. Vega, Proton line narrowing in solid-state nuclear magnetic resonance. New insights from windowed phase-modulated Lee–Goldburg sequence, J. Chem. Phys. 125 (2006) 124506.
[24] T. Terao, H. Miura, A. Saika, Measurements of the ^{13}C–^{1}H coupling constants in solid adamantane: resolution enhancement by multiple-pulse decoupling, J. Magn. Reson. 49 (1982) 365–367.
[25] B. Elena, G. de Paëpe, L. Emsley, Direct spectral optimization of proton–proton homonuclear dipolar decoupling in solid-state NMR, Chem. Phys. Lett. 398 (2004) 532–538.
[26] A. Lesage, D. Sakellariou, S. Hediger, B. Eléna, P. Charmont, S. Steuernagel, L. Emsley, Experimental aspects of proton NMR spectroscopy in solids using phase-modulated homonuclear dipolar decoupling, J. Magn. Reson. 163 (2003) 105–113.
[27] S. Paul, R.S. Thakur, M. Goswami, A.C. Sauerwein, S. Mamone, H. Förster, M.H. Levitt, P.K. Madhu, Supercycled homonuclear dipolar decoupling sequences in solid-state NMR, J. Magn. Reson. 197 (2009) 14–19.
[28] A.J. Vega, Controlling the effects of pulse transients and RF inhomegeneity in phase-modulated multiple-pulse sequences for homonuclear decoupling in solid-state NMR, J. Magn. Reson. 170 (2004) 22–41.
[29] K. Mao, M. Pruski, Directly and indirectly detected through-bond heteronuclear correlation solid-state NMR spectroscopy under fast MAS, J. Magn. Reson. 201 (2009) 165–174.
[30] M. Leskes, P.K. Madhu, S. Vega, A broad-banded *z*-rotation windowed phase-modulated Lee–Goldburg pulse sequence for ^{1}H spectroscopy in solid-state NMR, Chem. Phys. Lett. 447 (2007) 370–374.